AGU PUBLICATIONS

Geophysical Research Letters

RESEARCH LETTER
10.1002/2017GL073536

Key Points:
- Pacific SST anomalies are not required for widespread low annual streamflow across the western U.S.
- The 50% of western U.S. streamflow variability linked to midlatitude circulation and Pacific Northwest ridge

Supporting Information:
- Supporting Information S1
- Data Set S1
- Data Set S2
- Data Set S3

Correspondence to:
S. B. Malevich,
malevich@email.arizona.edu

Citation:
Malevich, S. B., and C. A. Woodhouse (2017), Pacific sea surface temperatures, midlatitude atmospheric circulation, and widespread interannual anomalies in western U.S. streamflow, *Geophys. Res. Lett.*, *44*, 5123–5132, doi:10.1002/2017GL073536.

Received 28 OCT 2016
Accepted 28 APR 2017
Accepted article online 3 MAY 2017
Published online 29 MAY 2017

Pacific sea surface temperatures, midlatitude atmospheric circulation, and widespread interannual anomalies in western U.S. streamflow

S. B. Malevich[1] **and C. A. Woodhouse**[2]

[1]Department of Geosciences, University of Arizona, Tucson, Arizona, USA, [2]School of Geography and Development, University of Arizona, Tucson, Arizona, USA

Abstract Widespread droughts can have considerable impact on western United States (U.S.) streamflow but causes related to moisture delivery processes are not yet fully understood. Here we examine western U.S. streamflow records to identify robust leading modes of interannual variability and their links to patterns of ocean and atmospheric circulation. The leading mode of streamflow variability, a pattern of west-wide streamflow anomalies, accounts for approximately 50% of variability and is associated with persistent high-pressure anomalies related to ridges off the Pacific North American coast. The second mode of variability accounts for approximately 25% of variability and is associated with ocean and atmospheric conditions in the tropical Pacific. Our results suggest that the leading mode of streamflow variability in the western U.S. is more strongly associated with internally driven midlatitude atmospheric variability than equatorial Pacific sea surface temperatures.

1. Introduction

Droughts affecting streamflow in multiple watersheds can have a profound impact on western United States (U.S.) water supplies. These droughts are often attributed, at least in part, to El Niño–Southern Oscillation (ENSO) variability in the equatorial Pacific [*Cayan et al.*, 1999; *Dettinger et al.*, 1998; *Redmond and Koch*, 1991; *Seager and Hoerling*, 2014; *Wise et al.*, 2014]. However, many drought events are not directly explained by ENSO alone. Some of the most spatially widespread events in the past century are linked with powerful, cool season, blocking atmospheric ridges in the midlatitudes. These features obstruct incoming moisture and are frequently associated with internal atmospheric variability. The unusually strong and widespread droughts in 1977 and 1934 are cited as examples of this [e.g., *Cook et al.*, 2014; *Hoerling et al.*, 2009; *Seager et al.*, 2014; *Diaz and Wahl*, 2015; *Wise*, 2016]. The 2014 California drought is also related to persistent ridging [*Cook et al.*, 2014; *Seager et al.*, 2015; *Teng and Branstator*, 2016; *S.-Y. Wang et al.*, 2014]. But these examples highlight the often tangled relationship between interacting ocean-atmosphere dynamics in the equatorial and midlatitude Pacific. For instance, the unusually strong atmospheric ridge during the 2014 drought has been linked with Pacific sea surface temperatures (SSTs) variability [e.g., *Herring et al.*, 2014; *Seager et al.*, 2015; *H. Wang et al.*, 2014; *Seager et al.*, 2014; *Teng and Branstator*, 2016; *S.-Y. Wang et al.*, 2014; *Hartmann*, 2015; *Swain*, 2015]. In the case of the 1934 drought, an unusually intense and persistent atmospheric ridge on the Pacific North American coast was briefly experienced during a longer drought associated with tropical Pacific SSTs [*Cook et al.*, 2014; *Herring et al.*, 2014; *Seager et al.*, 2008, 2005; *Schubert et al.*, 2004]. While equatorial Pacific SSTs have been shown to play an important role in triggering western U.S. drought, it is unclear how extensively and consistently the midlatitude atmosphere circulation—independent of tropical Pacific SSTs—can induce widespread drought and hydroclimate variability, particularly in western U.S. streamflow.

Our study approaches this issue with a focus on annual, western U.S. multibasin streamflow anomalies. Hydroclimate research has largely focused on precipitation, drought-related metrics, or streamflow in specific basins, but rarely on multibasin streamflow anomalies across the western U.S. Relative to other hydroclimate variables, the streamflow record has a number of unique and important characteristics. For example, an annual value from a streamflow gage is an integration of hydroclimate processes, spatially, across the extent of a basin or watershed, and temporally, through a full year. As such, it is a measure of the water supply in the basin resulting from these processes. Basin-scale water resources have played a vital role in the human and ecosystem development of the western U.S. Unlike most other hydroclimate variables, streamflow represents

a managed natural resource. In the Pacific Northwest, for example, 60–70% of energy supplies are produced by hydroelectric dams. Within the Columbia River basin, the U.S. Bureau of Reclamation, alone, manages an active capacity of over 22 km^3 of water spread across a network of 50 dams [*Reclamation*, 2016a]. To the south, a growing population of nearly 50 million people across seven U.S. states have come rely on water allocations from the Colorado River and its tributaries for municipal water needs [*Reclamation*, 2016a].

Many of the challenges in western U.S. water supplies are long-standing issues that are likely to be further confounded by climate change and natural hydroclimate variability that is poorly represented in the instrument record of the last century [*Meko et al.*, 2012; *Dettinger et al.*, 2015]. An improved understanding of the controls on annual water supply variability is critical for seasonal forecasts and long-term hydroclimate and streamflow projections. The state of ENSO is a widely used as a predictor in seasonal western U.S. forecast models because of its impact on the western U.S. and seasonal persistence [*Liu and Alexander*, 2007]. If the midlatitude ridging patterns that result in widespread streamflow deficits show consistent preference for one ENSO phase, or some other form of persistent SST variability, this might serve as a basis for improved forecasting and anticipating similar widespread streamflow drought and pluvial events in the future. However, if patterns of widespread streamflow variability are largely free of direct influence from ENSO or other persistent SST patterns, then the droughts and pluvials associated with these streamflow anomalies will generally be difficult, if not impossible to anticipate from seasonal forecasts.

Our main research question is how consistently are widespread water year (October–September) western U.S. streamflow anomalies associated with midlatitude atmospheric circulation, without significant and direct influence from equatorial Pacific SSTs? To address this question, we use principal components analysis (PCA) to identify the main patterns or modes of variability in western U.S. streamflow over the last century. The leading principal components (PCs) in streamflow are used to investigate variability in Pacific SSTs and atmospheric circulation corresponding to these main modes of variability.

2. Data

This study used water year (WY) streamflow data from the USGS Hydro-Climatic Data Network (HCDN) [*Lins*, 2012]. HCDN is a collection of stream gages intended for analysis of climatic trends and hydrologic variations with minimal influence from human activity. HCDN gages within the western U.S., from 104°W to 125°W, were selected for this study of which 169 gages with complete records from WY1975 to 2011 were used for analysis (Figure 1). We confirmed that patterns of variability from these 169 gages are reasonably robust through time by repeating our analysis on the subset of 65 gages with complete records from WY1950 to 2011 and also the subset of 16 gages with complete records from WY1925 to 2011. The results from the WY1925 and WY1975 periods are similar, suggesting that these patterns are reasonably robust (supporting information Figure S1 and Figure 1, respectively). Interestingly, the leading PCs from the WY1950 to 2011 subset differ from these results, showing a stronger ENSO-like influence in the leading PCs (supporting information Figure S2). We suspect that this difference is related to stronger spatial clustering in HCDN gages near the midcentury (see supporting information Figure S3). Results presented below refer to the WY1975–2011 streamflow analysis unless noted otherwise.

Global SSTs and Northern Hemisphere 500 mb geopotential height fields were used to identify climate variability associated with western U.S. streamflow. We used 500 mbar geopotential height data obtained from the Twentieth Century Reanalysis Version 2 (20CR) [*Compo et al.*, 2011]. The 500 mbar level is used because it is above the mountainous, higher elevations of the western U.S. SSTs used are from the NOAA Extended Reconstructed Sea Surface Temperature V3b (ERSST) [*Smith et al.*, 2008]. Both products have a 2° by 2° spatial resolution. The cool season is the primary period for moisture delivery into western U.S. river basins. Our analysis focuses on this seasonal moisture delivery as a primary influence on interannual streamflow variability. However, we examine all seasons to identify possible persistent or lagged relationships in geopotential height and SST fields influence. Annual season-averaged 500 mbar geopotential height anomalies are used for summer prior to the onset of the water year (June–August (JJA)), and for the fall (September–November), winter (December–February), and spring (March–May (MAM)) of the water year itself. These season averages were created from 20CR monthly average ensemble means. SST fields use the same seasons, averaged from monthly values but these values are linear-detrended anomalies. Note that there is considerably more uncertainty in the 20CR ensemble data prior to 1950 [*Compo et al.*, 2011]. To check against bias in 20CR and ERSST, we repeated analyses from 1983 to 2011 using HCDN streamflow data with geopotential height fields from

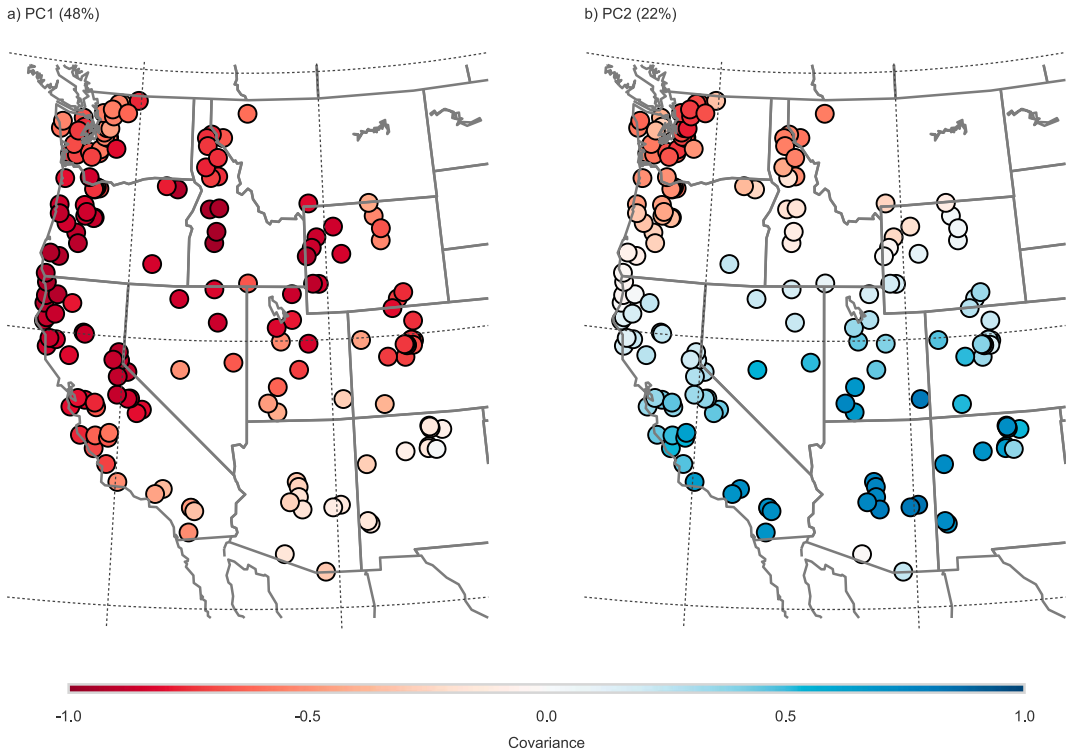

Figure 1. Spatial pattern of leading PCs mapped as covariance of streamflow PC1 and PC2 on standardized streamflow series (WY1975–2011). The percent value in figure title is the percent of streamflow variability accounted for by the PC.

ERA-Interim reanalysis [*Dee et al.*, 2011; *European Centre for Medium-Range Weather Forecasts*, 2012] and SST fields from Optimum Interpolation Sea Surface Temperature analysis V2 [*Reynolds et al.*, 2007]. The results were comparable to that produced with 20CR and ERSST.

3. Methods

Each annual streamflow series was transformed into standardized values from the common period of analysis. This standardization addresses potentially differing streamflow distribution scales, shapes, and spreads. We were concerned that these differences might otherwise bias extreme values in a PCA conducted on streamflow series from different western U.S. basins. Values were standardized by fitting each streamflow series to a gamma distribution and then inverting the corresponding probabilities to a Gaussian distribution. In short, this transformation is similar to the Standardized Precipitation Index [*McKee et al.*, 1993] for precipitation, though applied to streamflow data. We used a Kolmogorov-Smirnov goodness-of-fit test for each gage against a fitted gamma distribution. Only one gage in California did not reject the null hypothesis that the distribution is identical to a fitted gamma distribution ($\alpha = 0.05$). In addition, we repeated this study's analysis using a Z score standardization of streamflow. Despite our concern, Z score standardization produced similar results.

PCA was based on singular value decomposition of the standardized streamflow covariance matrix. This PCA allowed us to define the dominant patterns of variability in western U.S. streamflow, with each component being independent (i.e., orthogonal) from other components. Significant, leading PCs were identified by evaluating the explained variance and separation from other components [*North et al.*, 1982]. The PCs were standardized to unit variance. The leading empirical orthogonal functions, the spatial expression of the leading PC pattern, were mapped by plotting the covariance of a PC with the standardized streamflow data. See *Wilks* [2006] for a review of these methods.

The leading patterns of streamflow variability were used to identify relationships with seasonal SST and 500 mbar geopotential height fields using two methods. First, point-correlation maps were generated to identify simple linear relationships between the leading streamflow PC time series and the SST and geopotential

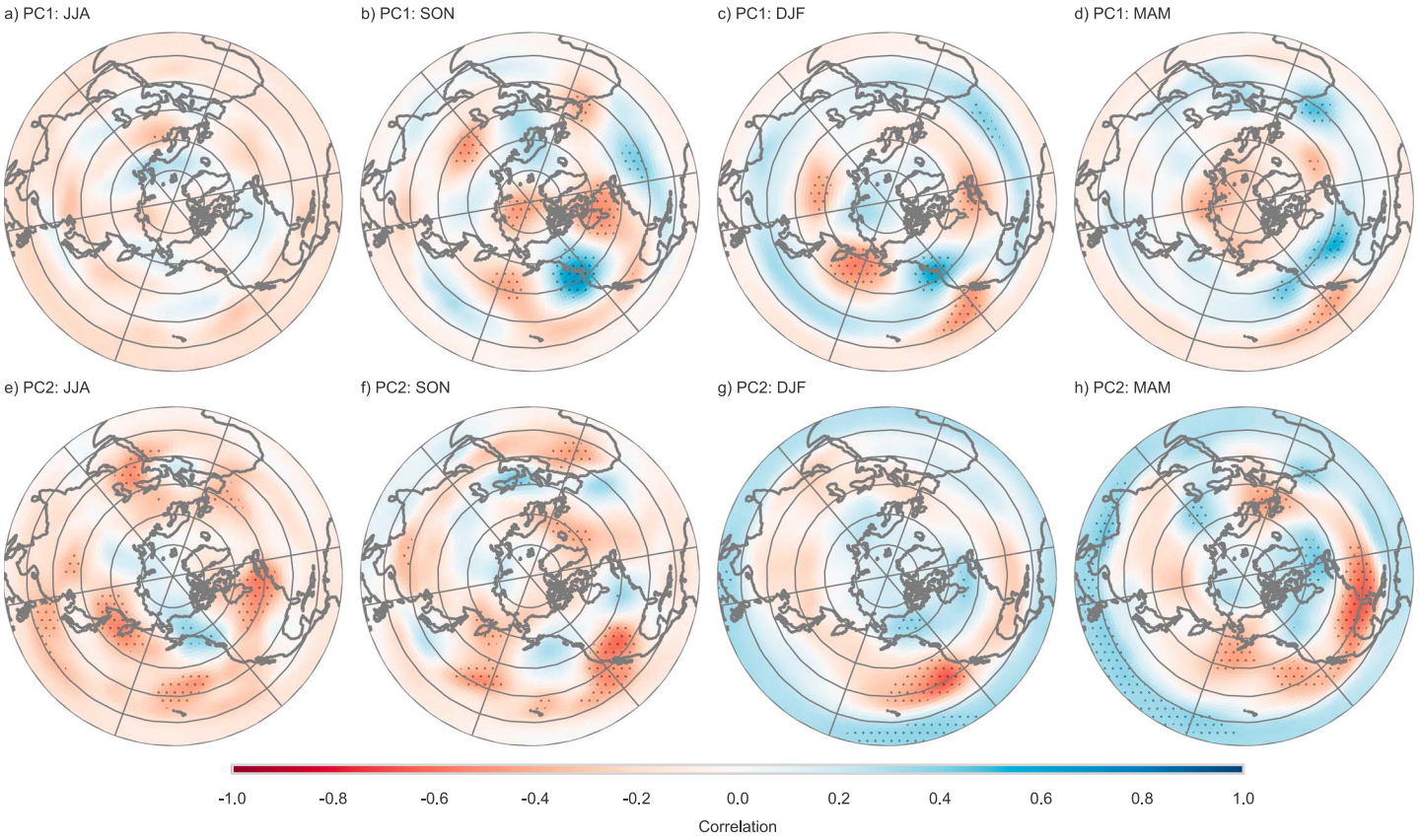

Figure 2. (a–h) Point correlation map of streamflow PC1 and PC2 on 500 mbar geopotential height anomaly fields for each season in the Northern Hemisphere (WY1975–2011). Stippled areas show local statistical significance ($\alpha = 0.05$).

height fields. Pearson product-moment correlation coefficients for each leading PC and field grid point were mapped and local, statistical significance tested ($\alpha = 0.05$).

Point-correlation maps were supplemented with nonparametric composite analysis maps. These maps identify areas in a SST or geopotential height field that exhibit statistically significant mean differences between positive and negative signs of a streamflow PC time series. These maps were created for each leading streamflow PC for each climate field. Differences between the patterns for years with negative and positive PC loadings were tested using Welch's unequal variance *t* test for each grid point in the field. This procedure tests against the null hypothesis that the two composite samples have equal means while accounting for the variance of each sample. Grid points that exhibited consistent changes with streamflow PCs, rejecting the null hypothesis ($\alpha = 0.05$), were mapped.

Our analysis was performed in Python using several Open Source scientific software libraries [*Hunter*, 2007; *van der Walt et al.*, 2011; *Dawson*, 2016]. Code used in our data collection and analysis is available online (https://github.com/brews/riverpca) or by request from the corresponding author.

4. Results and Discussion

Interannual western U.S. streamflow is characterized by two leading and well-separated patterns of variability in the past century (Figure 1). The leading pattern, or principal component (PC1), accounts for approximately one half of streamflow variability (48%), while the second pattern (PC2) accounts for approximately one quarter of variability (22%). A linear combination of these two patterns accounts for roughly three quarters of the variability in standardized streamflow. Time series of PC1 and PC2 are shown in supporting information Figure S4. The two leading PCs for streamflow are including in supporting information Data Set S1.

The leading patterns of streamflow variability have distinct spatial characteristics that relate to cool season moisture delivery. PC1 is associated with widespread flow anomalies of the same sign across western U.S.

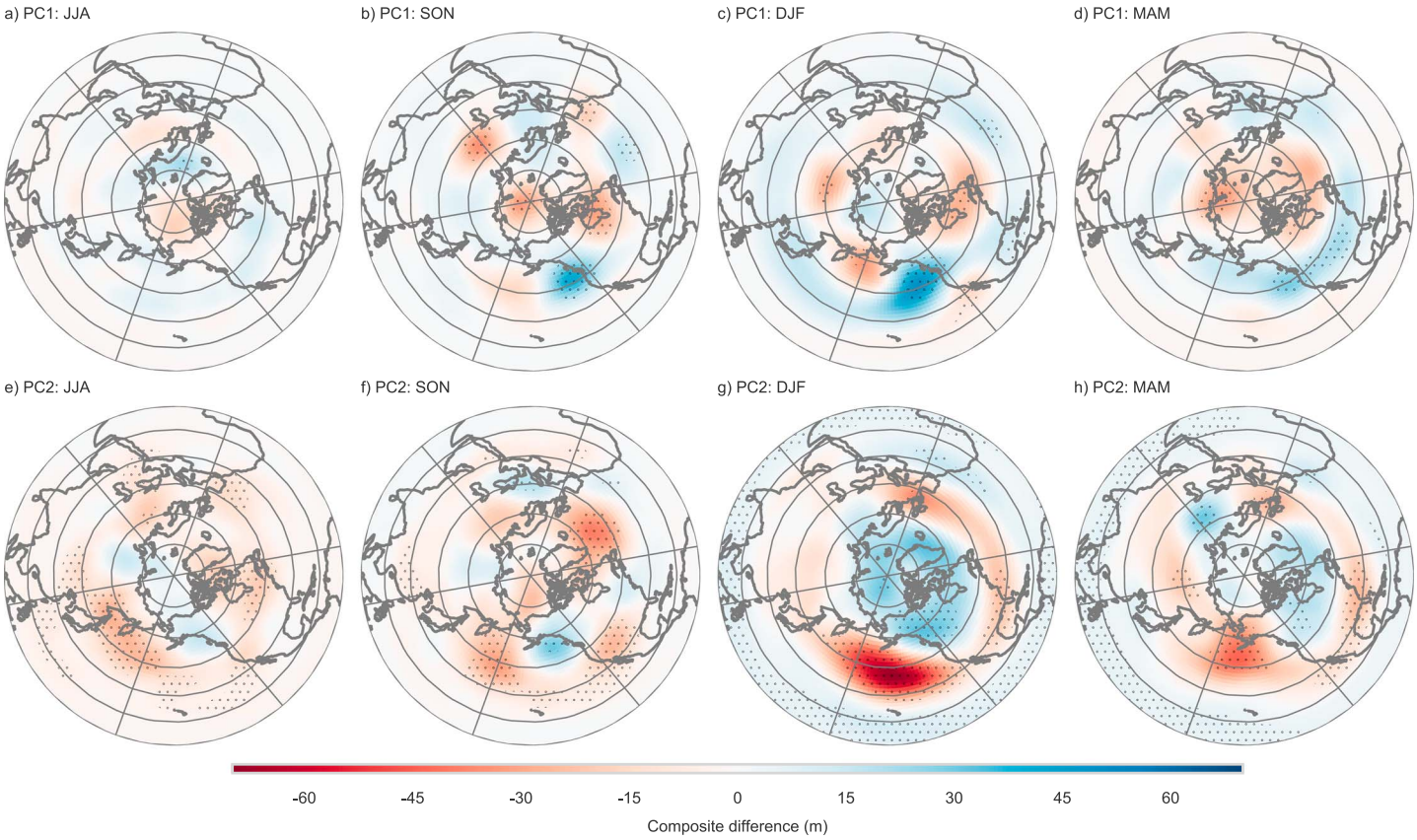

Figure 3. (a–h) Composite mean difference 500 mbar geopotential height anomaly for each season. This difference is the composite of positive streamflow PC years minus negative PC years for PC1 and PC2. Stippled areas show composite means with local statistical significance ($\alpha = 0.05$).

streamflow (Figure 1a). This widespread single-sign covariability has been noted previously in western U.S. streamflow, snowpack, and coastal precipitation analyses [*McGuirk*, 1982; *Cayan and Peterson*, 1989; *Lins*, 1997; *McCabe and Dettinger*, 2002]. The spatial expression of PC2 (Figure 1b) is a contrasting north-south seesaw or dipole pattern, a well-established characteristic of the western U.S. linear climate response to ENSO in the cool season [*Dettinger et al.*, 1998; *Wise*, 2010]. These two streamflow patterns and their climate relationships are replicated in the WY1925–2011 PCA. Analysis for this longer PCA is available in the supporting information.

4.1. Midlatitude Atmospheric Circulation and Blocking Pressure Anomalies in PC1

The correlations between the leading pattern of streamflow variability (PC1) and 500 mbar geopotential height from fall through spring (Figures 2b–2d) reflects the pattern's association with cool season synoptic-scale atmospheric circulation. No significant, organized relationship is evident in the summer correlation map (Figure 2a). During fall and winter, the significant positive correlations over the North American Cordillera and northwest coast are flanked by negative correlations near the Aleutian Islands and eastern North America, reflecting midlatitude atmospheric circulation wave-train dynamics (Figures 2b and 2c). The area of significant positive correlation near the northwest U.S., specifically, is found in fall (Figure 2b), winter (Figure 2c), and spring (Figure 2d). This suggests that widespread low streamflow is associated with anomalously high pressure characteristic of a persistent ridge. This is a pressure anomaly which can preferentially block, separate, or suppress incoming cool season moisture from the Pacific. The high PC1 value in 1977, a year with an intense ridge and widespread streamflow drought, is an example of this (see supporting information Figure S4a). Inversely, negative pressure anomalies over this area are associated with widespread high streamflow anomalies. This relationship with geopotential height is inverted farther to the south near the Baja California peninsula in winter and spring (Figures 2c and 2d). The consistency and strength of the anomalies near the northwest U.S. is further emphasized in the PC1 composite test for 500 mbar geopotential heights from fall through spring (Figures 3b–3d), demonstrating statistically significant geopotential height differences

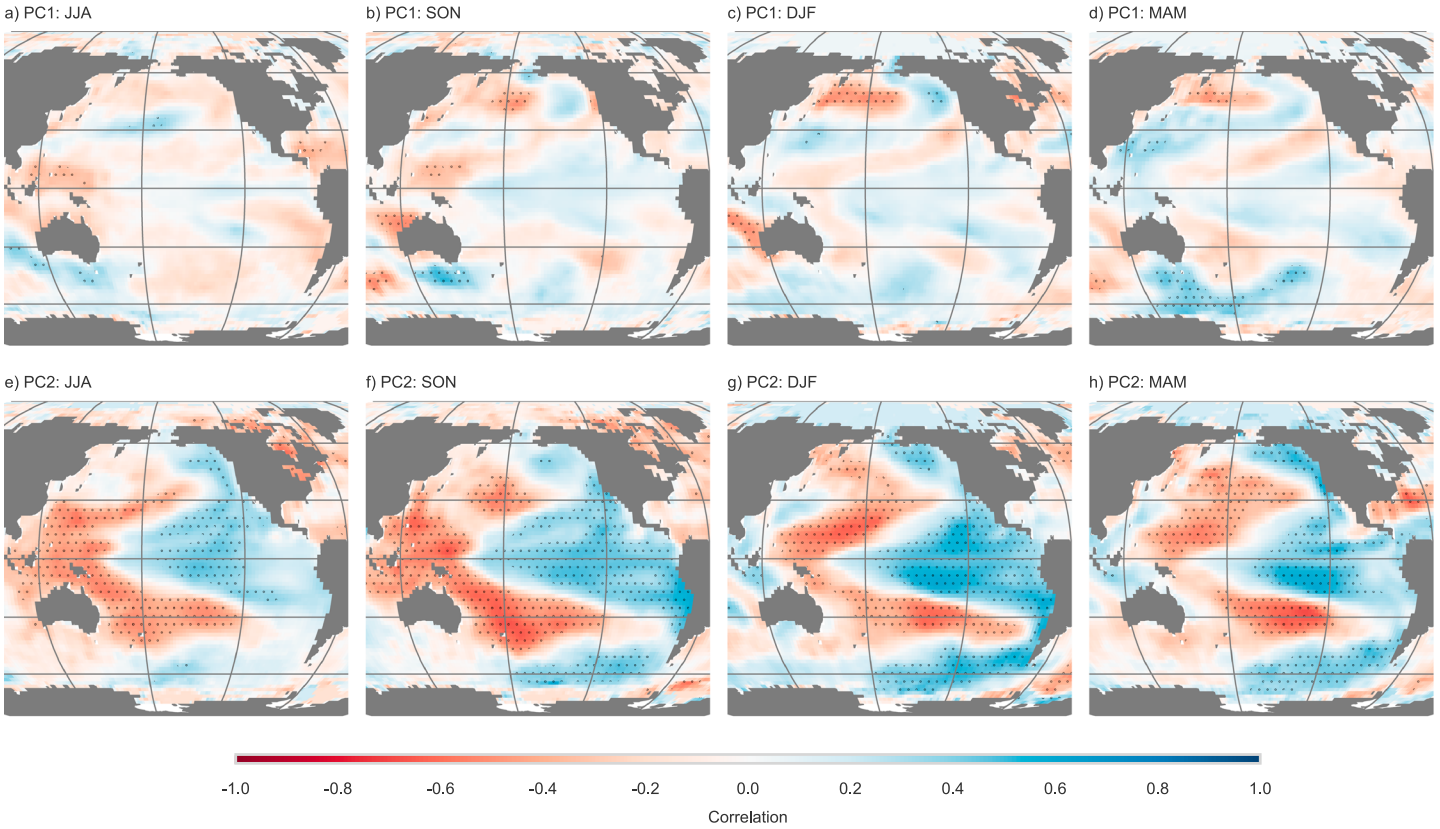

Figure 4. (a–h) Point correlation map of streamflow PC1 and PC2 on detrended SST anomaly fields for each season (WY1975–2011). Stippled areas show local statistical significance ($\alpha = 0.05$).

between positive and negative PC1 years (i.e., years of widespread high and low streamflow anomalies). These composite maps show significance near the North American Pacific coast, but not near the semipermanent Aleutian low.

The widespread covariability in streamflow has been associated with the semipermanent Aleutian low [*Cayan and Peterson*, 1989; *Lins*, 1997], and this is shown in our results: a center of negative correlation near the Aleutian islands in fall and winter (Figures 2b and 2c), but not spring (Figure 2d). Interestingly, geopotential height anomalies at the Aleutian Islands do not show widespread significant difference between positive and negative PC1 years in any season (Figures 3a–3d). This suggests that a relationship does exist with pressure anomalies near the Aleutian Islands; however, widespread variability in western U.S. streamflow may have a more immediate and consistent relationship with the anomalies relating to North American Pacific coast ridging behavior.

The leading pattern of streamflow variability does not have widespread significant correlations with SSTs (Figures 4a–4d), especially when compared to PC2 (Figures 2e–2h). Positive North Pacific SST correlations with PC1 are found in the winter (Figure 4c) along the coast of southern Alaska and British Columbia with opposite-sign SST correlations from the central North Pacific to northeast Asia. More generally, negative SST correlations in the central North Pacific are found in fall, winter, and spring (Figures 4b–4d). This pattern hints at a possible relation between west-wide streamflow and the leading mode of variability for North Pacific SST [*Mantua and Hare*, 2002]. This relationship has been proposed for western U.S. snowpack variability [*McCabe and Dettinger*, 2002] and in earlier streamflow studies [e.g., *Tootle et al.*, 2005; *Tootle and Piechota*, 2006; *Sagarika et al.*, 2016]. However, the fall-through-spring SST composite-test map for PC1 shows no corresponding widespread areas of the North Pacific with statistically significant differences between the years of positive and negative PC1 values (Figures 5b–5d), though PC1 in the WY1925 PCA does have an area of significance in winter (supporting information Figure S8). PC1 may be influenced by North Pacific SSTs, but our

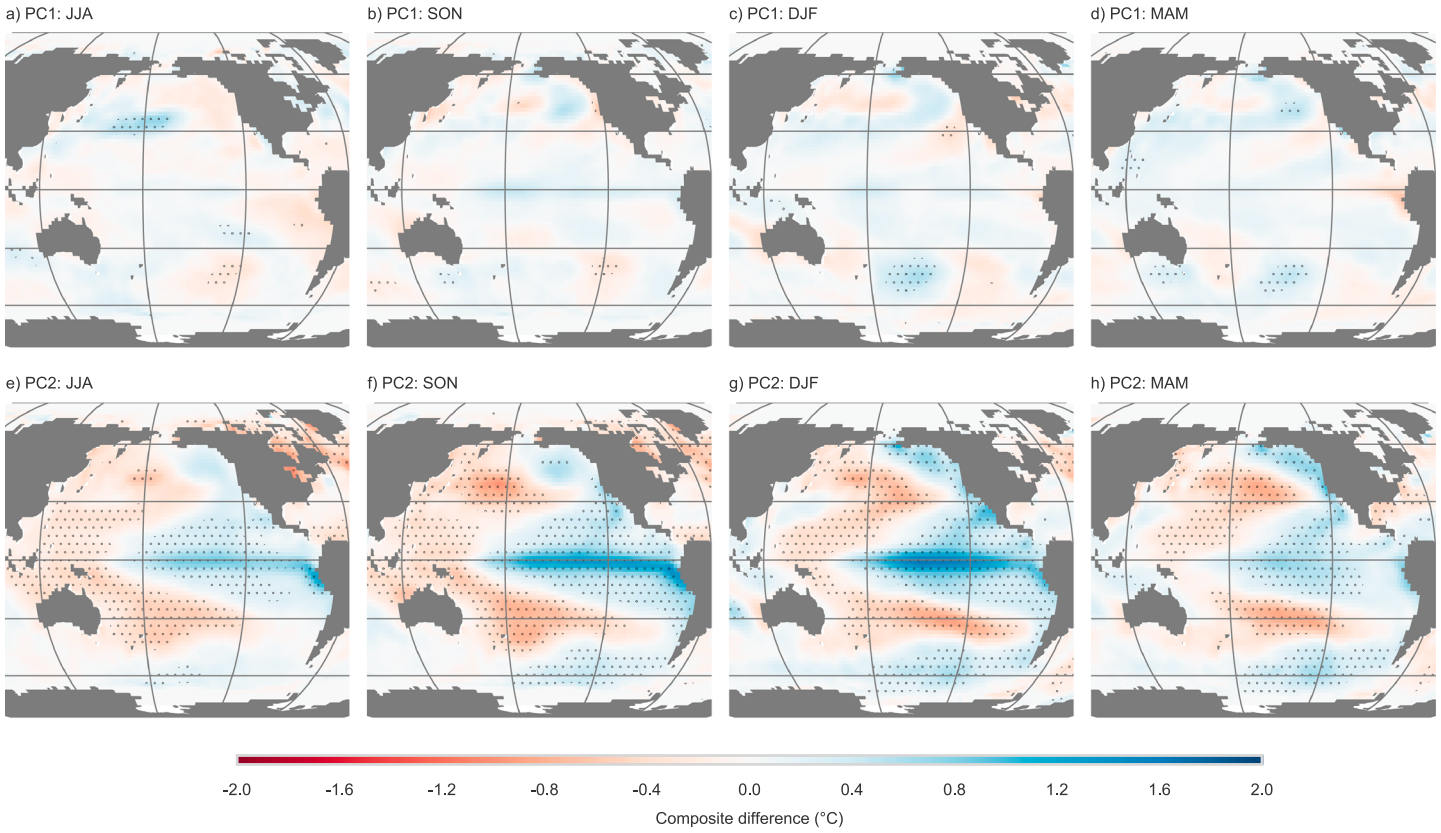

Figure 5. (a–h) Composite mean difference detrended SST anomaly for each season. This difference is the composite of positive streamflow PC years minus negative PC years for PC1 and PC2. Stippled areas show composite means with local statistical significance ($\alpha = 0.05$).

results suggest that organized SSTs in the North Pacific are not a consistent driver of interannual covariability in streamflow across the western U.S.

4.2. ENSO Teleconnection in PC2

Point-correlation maps of the second leading pattern of streamflow variability with winter 500 mbar geopotential height anomalies show an ENSO-like influence with significant correlations to higher latitudes near Alaska and northwest Canada, and a wide area of opposite sign correlation off the California coast (Figure 2g). Correlation maps with winter SST anomalies show significant correlations across the equatorial Pacific that extend symmetrically into the higher latitudes (Figure 4g). This ENSO-like pattern is also found in the PC2 composite maps for SST anomalies in all seasons (Figures 5e–5h).

Geopotential height correlation maps show areas of significant correlation establishing and sustaining a linear relationship with PC2, leading and lagging winter by several months (Figures 2e–2h). A similar lag-lead relationship is found with SST anomalies (Figures 4e–4h). The SST correlations cover considerably more area through each of the seasons (Figures 4e–4h). This relationship begins as early as summer (JJA) and continues through spring (MAM). Explaining approximately one quarter of the streamflow variability, ENSO state is clearly important for seasonal forecasts of streamflow, yet potentially limited as a predictor when used by itself.

4.3. Implications for Widespread Streamflow Anomalies

Our results show that roughly 50% of interannual streamflow variability in the western U.S. can be expressed as widespread streamflow anomalies without consistent need for Pacific SST forcing. Orthogonal to this pattern, approximately 25% of interannual streamflow variability is linked to the well-established western U.S. hydroclimate response to ENSO teleconnections. Rather than stressing the role of the ENSO or North Pacific multidecadal variability [e.g., *Tootle et al.*, 2005; *Sagarika et al.*, 2016], our results stress the potential influence of internal climate variability and the role of persistent coastal-ridge pressure anomalies in the eastern North Pacific as a consistent and direct source of cohesion for multibasin streamflow variability. These mechanisms

closely correspond to those discussed in recent drought studies [e.g., *Cook et al.*, 2014; *Seager and Hoerling*, 2014; *Teng and Branstator*, 2016; *Wise*, 2016]. We show that these two streamflow patterns have likely been a robust characteristic of streamflow variability through to the early half of the twentieth century.

These results suggest that widespread interannual streamflow anomalies may be especially difficult to anticipate with seasonal hydroclimate forecasts because the widespread streamflow variability in PC1 is not consistently related to ENSO variability nor does it show strong and widespread seasonal lag-lead correlations with Pacific SSTs to the extent that we have seen with PC2's reflection of ENSO-like teleconnections. In contrast, ENSO-related anomalies in PC2 may be more readily forecasted, but this variability is associated with approximately one quarter of the variability in western U.S. streamflow.

Years with extremely widespread and intense streamflow drought relating to persistent coastal ridges, such as 1977, can be interpreted as an extreme expression of PC1, which we associate with semipermanent 500 mbar ridging along the Pacific coast and a deepening of Aleutian low anomalies. Future climate change is projected to significantly shift semipermanent air masses and midlatitude storm tracks [e.g., *Yin*, 2005; *Lu et al.*, 2007; *Scheff and Frierson*, 2012; *Langenbrunner et al.*, 2015; *Choi et al.*, 2016]. If these shifts in North Pacific atmospheric circulation are realized, it could change the way that semipermanent air masses impact widespread streamflow anomalies. Unfortunately, it may be challenging to project these changes and how they will affect water management since there are still a number of outstanding uncertainties in climate model projections [e.g., *Reclamation*, 2016b], particularly in the eastern North Pacific [e.g., *Langenbrunner et al.*, 2015; *Choi et al.*, 2016].

5. Conclusion

Our analysis suggests that widespread western U.S. streamflow anomalies are most strongly associated with midlatitude atmospheric circulation relating to persistent atmospheric ridges, independent of direct interaction from ENSO and equatorial Pacific SSTs. This result appears to be a consistent characteristic of the instrumental streamflow record in the past century, accounting for roughly one half of the variance in western U.S. annual streamflow. Roughly one quarter of streamflow variability is associated with ENSO-like teleconnections. Because ENSO-state provides forecasting skill, this influence on streamflow may be anticipated seasons in advance. However, ENSO-driven streamflow anomalies can be complicated by significant and more spatially widespread influence from midlatitude atmospheric circulation, as seen in the extreme 1977 drought. This western U.S.-wide influence from midlatitude circulation is not as strongly associated with Pacific SSTs and will likely be a challenge to anticipate in seasonal hydroclimate forecasts. These patterns in streamflow may change with shifting North Pacific atmospheric circulation under future climate change, though we do not see evidence of these changes in our analysis of the past century.

Acknowledgments
Thanks to Joellen Russell, Elizabeth Ritchie, Chris Castro, Kevin Anchukaitis, Andrew Comrie, and Dave Meko. Thanks also to our anonymous reviewers for their feedback. NOAA ERSST and 20th Century Reanalysis data were provided by the NOAA/OAR/ESRL PSD, Boulder, Colorado, USA (http://www.esrl.noaa.gov/psd/). This research was supported by the U.S. Bureau of Reclamation WaterSmart program (agreement R11 AP 81 457).

References

Cayan, D. R., and D. H. Peterson (1989), The influence of North Pacific atmospheric circulation on streamflow in the west, in *Aspects of Climate Variability in the Pacific and the Western Aimericas*, edited by D. H. Peterson, pp. 375–397, AGU, Washington, D. C. doi:10.1029/GM055p0375.

Cayan, D. R., K. T. Redmond, and L. G. Riddle (1999), ENSO and hydrologic extremes in the western United States, *J. Clim.*, *12*(9), 2881–2893, doi:10.1175/1520-0442(1999)012<2881:EAHEIT>2.0.CO;2.

Choi, J., J. Lu, S.-W. Son, D. M. W. Frierson, and J.-H. Yoon (2016), Uncertainty in future projections of the North Pacific subtropical high and its implication for California winter precipitation change, *J. Geophys. Res. Atmos.*, *121*, 795–806, doi:10.1002/2015JD023858.

Compo, G. P., et al. (2011), The twentieth century reanalysis project, *Q. J. R. Meteorol. Soc.*, *137*(654), 1–28, doi:10.1002/qj.776.

Cook, B. I., R. Seager, and J. E. Smerdon (2014), The worst North American drought year of the last millennium: 1934, *Geophys. Res. Lett.*, *41*(20), 7298–7305, doi:10.1002/2014GL061661.

Dawson, A. (2016), EOFS: A library for EOF analysis of meteorological, oceanographic, and climate data, *J. Open Res. Softw.*, *4*(1), e14, doi:10.5334/jors.122.

Dee, D. P., et al. (2011), The ERA-Interim reanalysis: Configuration and performance of the data assimilation system, *Q. J. R. Meteorol. Soc.*, *137*(656), 553–597, doi:10.1002/qj.828.

Dettinger, M., B. Udall, and A. Georgakakos (2015), Western water and climate change, *Ecol. Appl.*, *25*(8), 2069–2093, doi:10.1890/15-0938.1.

Dettinger, M. D., D. R. Cayan, H. F. Diaz, and D. M. Meko (1998), North-south precipitation patterns in western North America on interannual-to-decadal timescales, *J. Clim.*, *11*(12), 3095–3111, doi:10.1175/1520-0442(1998)011<3095:NSPPIW>2.0.CO;2.

Diaz, H. F., and E. R. Wahl (2015), Recent california water year precipitation deficits: A 440-year perspective, *J. Clim.*, *28*(12), 4637–4652, doi:10.1175/JCLI-D-14-00774.1.

European Centre for Medium-Range Weather Forecasts (2012), *ERA-Interim Project, Monthly Means*, ECMWF, Reading, U. K.

Hartmann, D. L. (2015), Pacific sea surface temperature and the winter of 2014, *Geophys. Res. Lett.*, *42*(6), 1894–1902, doi:10.1002/2015GL063083.

Herring, S. C., M. P. Hoerling, T. C. Peterson, and P. A. Stott (2014), Explaining extreme events of 2013 from a climate perspective, *Bull. Am. Meteorol. Soc.*, *95*, S1—S104.
Hoerling, M., X.-W. Quan, and J. Eischeid (2009), Distinct causes for two principal U.S. droughts of the 20th century, *Geophys. Res. Lett.*, *36*, L19708, doi:10.1029/2009GL039860.
Hunter, J. D. (2007), Matplotlib: A 2D graphics environment, *Comput. Sci. Eng.*, *9*(3), 90–95, doi:10.1109/MCSE.2007.55.
Langenbrunner, B., J. D. Neelin, B. R. Lintner, and B. T. Anderson (2015), Patterns of precipitation change and climatological uncertainty among CMIP5 models, with a focus on the midlatitude Pacific storm track, *J. Clim.*, *28*(19), 7857–7872, doi:10.1175/JCLI-D-14-00800.1.
Lins, H. F. (1997), Regional streamflow regimes and hydroclimatology of the United States, *Water Resour. Res.*, *33*(7), 1655–1667, doi:10.1029/97WR00615.
Lins, H. F. (2012), USGS Hydro-Climatic Data Network 2009 (HCDN-2009): U.S. Geological Survey Fact Sheet 2012–3047. [Available at https://pubs.usgs.gov/fs/2012/3047/.]
Liu, Z., and M. Alexander (2007), Atmospheric bridge, oceanic tunnel, and global climatic teleconnections, *Rev. Geophys.*, *45*, RG2006, doi:10.1029/2005RG000172.
Lu, J., G. A. Vecchi, and T. Reichler (2007), Expansion of the Hadley cell under global warming, *Geophys. Res. Lett.*, *34*, L06805, doi:10.1029/2006GL028443.
Mantua, N., and S. Hare (2002), The Pacific Decadal Oscillation, *J. Oceanogr.*, *58*(1), 35–44, doi:10.1023/A:1015820616384.
McCabe, G. J., and M. D. Dettinger (2002), Primary modes and predictability of year-to-year snowpack variations in the western United States from teleconnections with Pacific Ocean climate, *J. Hydrometeorol.*, *3*(1), 13–25, doi:10.1175/1525-7541(2002)003<0013:PMAPOY>2.0.CO;2.
McGuirk, J. P. (1982), A century of precipitation variability along the Pacific coast of North America and its impact, *Clim. Change*, *4*(1), 41, doi:10.1007/BF02423312.
McKee, T. B., N. J. Doesken, and J. Kleist (1993), The relationship of drought frequency and duration to time scales, in *Proceedings of the 8th Conference on Applied Climatology, 22*, vol. 17, pp. 179–183, Am. Meteorol. Soc., Boston, Mass.
Meko, D. M., C. A. Woodhouse, and K. Morino (2012), Dendrochronology and links to streamflow, *J. Hydrol.*, *412–413*, 200–209, doi:10.1016/j.jhydrol.2010.11.041.
North, G. R., T. L. Bell, R. F. Cahalan, and F. J. Moeng (1982), Sampling errors in the estimation of empirical orthogonal functions, *Mon. Weather Rev.*, *110*(7), 699–706, doi:10.1175/1520-0493(1982)110<0699:SEITEO>2.0.CO;2.
Reclamation (Bureau of Reclamation), (2016a), SECURE Water Act Section 9503(c)—Reclamation climate change and water. Prepared for United States Congress, *Tech. Rep., U.S. Bureau of Reclamation*, Policy and Administration, Denver, Colo.
Reclamation (Bureau of Reclamation), (2016b), West-wide climate risk assessments: Hydroclimate projections, *Tech. Memorandum 86-68210-2016-01*, U.S. Bureau of Reclamation, Denver, Colo.
Redmond, K. T., and R. W. Koch (1991), Surface climate and streamflow variability in the western United States and their relationship to large-scale circulation indices, *Water Resour. Res.*, *27*(9), 2381–2399, doi:10.1029/91WR00690.
Reynolds, R. W., T. M. Smith, C. Liu, D. B. Chelton, K. S. Casey, and M. G. Schlax (2007), Daily high-resolution-blended analyses for sea surface temperature, *J. Clim.*, *20*(22), 5473–5496, doi:10.1175/2007JCLI1824.1.
Sagarika, S., A. Kalra, and S. Ahmad (2016), Pacific Ocean SST and Z500 climate variability and western U.S. seasonal streamflow, *Int. J. Climatol.*, *36*(3), 1515–1533, doi:10.1002/joc.4442.
Scheff, J., and D. Frierson (2012), Twenty-first-century multimodel subtropical precipitation declines are mostly midlatitude shifts, *J. Clim.*, *25*(12), 4330–4347, doi:10.1175/JCLI-D-11-00393.1.
Schubert, S. D., M. J. Suarez, P. J. Pegion, R. D. Koster, and J. T. Bacmeister (2004), On the cause of the 1930s dust bowl, *Science*, *303*(5665), 1855–1859, doi:10.1126/science.1095048.
Seager, R., and M. Hoerling (2014), Atmosphere and ocean origins of North American droughts, *J. Clim.*, *27*(12), 4581–4606, doi:10.1175/JCLI-D-13-00329.1.
Seager, R., Y. Kushnir, C. Herweijer, N. Naik, and J. Velez (2005), Modeling of tropical forcing of persistent droughts and pluvials over western North America: 1856–2000, *J. Clim.*, *18*(19), 4065–4088, doi:10.1175/JCLI3522.1.
Seager, R., Y. Kushnir, M. Ting, M. Cane, N. Naik, and J. Miller (2008), Would advance knowledge of 1930s SSTs have allowed prediction of the dust bowl drought?, *J. Clim.*, *21*(13), 3261–3281, doi:10.1175/2007JCLI2134.1.
Seager, R., M. Hoerling, S. Schubert, H. Wang, B. Lyon, A. Kumar, J. Nakamura, and N. Henderson, (2014), Causes and predictability of the 2011 to 2014 California drought, Tech. Rep., National Oceanic and Atmospheric Administration, Washington, D. C.
Seager, R., M. Hoerling, S. Schubert, H. Wang, B. Lyon, A. Kumar, J. Nakamura, and N. Henderson (2015), Causes of the 2011–14 California drought, *J. Clim.*, *28*(18), 6997–7024, doi:10.1175/JCLI-D-14-00860.1.
Smith, T. M., R. W. Reynolds, T. C. Peterson, and J. Lawrimore (2008), Improvements to NOAA's historical merged land-ocean surface temperature analysis (1880–2006), *J. Clim.*, *21*(10), 2283–2296, doi:10.1175/2007JCLI2100.1.
Swain, D. L. (2015), A tale of two California droughts: Lessons amidst record warmth and dryness in a region of complex physical and human geography, *Geophys. Res. Lett.*, *42*, 9999–10,003, doi:10.1002/2015GL066628.
Teng, H., and G. Branstator (2016), Causes of extreme ridges that induce California droughts, *J. Clim.*, *30*(4), 1477, doi:10.1175/JCLI-D-16-0524.1.
Tootle, G. A., and T. C. Piechota (2006), Relationships between Pacific and Atlantic ocean sea surface temperatures and U.S. streamflow variability, *Water Resour. Res.*, *42*(7), W07411, doi:10.1029/2005WR004184.
Tootle, G. A., T. C. Piechota, and A. Singh (2005), Coupled oceanic-atmospheric variability and U.S. streamflow, *Water Resour. Res.*, *41*(12), W12408, doi:10.1029/2005WR004381.
van der Walt, S., S. C. Colbert, and G. Varoquaux (2011), The NumPy array: A structure for efficient numerical computation, *Comput. Sci. Eng.*, *13*(2), 22–30, doi:10.1109/MCSE.2011.37.
Wang, H., S. Schubert, R. Koster, Y.-G. Ham, and M. Suarez (2014), On the role of SST forcing in the 2011 and 2012 extreme U.S. heat and drought: A study in contrasts, *J. Hydrometeorol.*, *15*(3), 1255–1273, doi:10.1175/JHM-D-13-069.1.
Wang, S.-Y., L. Hipps, R. R. Gillies, and J.-H. Yoon (2014), Probable causes of the abnormal ridge accompanying the 2013–2014 California drought: ENSO precursor and anthropogenic warming footprint, *Geophys. Res. Lett.*, *41*, 3220–3226, doi:10.1002/2014GL059748.
Wilks, D. (2006), *Statistical Methods in the Atmospheric Sciences*, 2nd ed., Int. Geophys. Ser., Academic Press, London.
Wise, E. K. (2010), Spatiotemporal variability of the precipitation dipole transition zone in the western United States, *Geophys. Res. Lett.*, *37*, L07706, doi:10.1029/2009GL042193.

Wise, E. K. (2016), Five centuries of U.S. West Coast drought: Occurrence, spatial distribution, and associated atmospheric circulation patterns, *Geophys. Res. Lett.*, *43*, 4539–4546, doi:10.1002/2016GL068487.

Wise, E. K., M. L. Wrzesien, M. P. Dannenberg, and D. L. McGinnis (2014), Cool-season precipitation patterns associated with teleconnection interactions in the United States, *J. Appl. Meteorol. Climatol.*, *54*(2), 494–505, doi:10.1175/JAMC-D-14-0040.1.

Yin, J. H. (2005), A consistent poleward shift of the storm tracks in simulations of 21st century climate, *Geophys. Res. Lett.*, *32*, L18701, doi:10.1029/2005GL023684.